Hindawi Publishing Corporation
Advances in Materials Science and Engineering
Volume 2015, Article ID 485626, 7 pages
http://dx.doi.org/10.1155/2015/485626

Research Article

Ostwald Ripening Process of Coherent β' Precipitates during Aging in $Fe_{0.75}Ni_{0.10}Al_{0.15}$ and $Fe_{0.74}Ni_{0.10}Al_{0.15}Cr_{0.01}$ Alloys

N. Cayetano-Castro, M. L. Saucedo-Muñoz, H. J. Dorantes-Rosales, Jorge L. Gonzalez-Velazquez, J. D. Villegas-Cardenas, and V. M. Lopez-Hirata

Instituto Politécnico Nacional (ESIQIE-CNMN), Apartado Postal 118-556, 07051 Mexico, DF, Mexico

Correspondence should be addressed to V. M. Lopez-Hirata; vlopezhi@prodigy.net.mx

Received 26 September 2014; Revised 16 December 2014; Accepted 6 January 2015

Academic Editor: Jörg M. K. Wiezorek

The Ostwald ripening process was studied in $Fe_{0.75}Ni_{0.10}Al_{0.15}$ and $Fe_{0.74}Ni_{0.10}Al_{0.15}Cr_{0.01}$ alloys after aging at 750, 850, and 950°C for different times. The microstructural evolution shows a rounded cube morphology (Fe, Ni)Al β' precipitates aligned in the ferrite matrix, which changes to elongated plates after prolonged aging. The variation of the equivalent radii of precipitates with time follows the modified Lifshitz-Slyozov-Wagner theory for diffusion-controlled coarsening. Thermo-Calc analysis shows that the chromium content is richer in the matrix than in the precipitates which causes higher hardness and coarsening resistance in the aged $Fe_{0.74}Ni_{0.10}Al_{0.15}Cr_{0.01}$ alloy.

1. Introduction

The mechanical properties of precipitation hardened alloys are closely related to the morphology, spatial distribution, volumetric fraction, and average radius of the precipitated particles in the phase matrix. These microstructural characteristics can be controlled by means of heat treatments; however, they are also modified during the operation of industrial components at high temperatures for prolonged times. The Ostwald ripening process is a metallurgical phenomenon which takes place at high temperatures and consists of the dissolution of small precipitates and subsequent mass transfer to the larger precipitates during the heating of alloys [1]. The Lifshitz-Slyozov-Wagner (LSW) theory for diffusion-controlled coarsening [2] predicts a coarsening growth kinetics with a time dependent on $t^{1/3}$ considering the spherical precipitates without elastic interaction with the phase matrix and volume fraction close to zero. There are several modified LSW theories for diffusion-controlled coarsening [3–6] which incorporated higher volume fractions and the precipitate morphology different from spheres, as well as multicomponent alloys. Nevertheless, the temporal power law of $t^{1/3}$ is sustained in all of the above cases, but the time-independent precipitate size distribution of LSW theory becomes broader and more symmetric with the increase in volume fraction.

The mechanical strength at high temperatures in Fe-Ni-Al alloys is mainly based on the presence of coherent (NiAl type) β' precipitates with a B2 (CsCl) crystalline structure dispersed in the ferrite matrix [7]. This intermetallic compound precipitate is responsible for the precipitation hardening in different alloy systems such as PH stainless steels, Nitralloy, and Fe-Cr-Ni-Al based alloys [8]. The coarsening resistance of these precipitates is an important factor to keep its mechanical strength at high temperatures in these alloys. One way for improving the coarsening resistance is by the addition of alloying elements to these alloys in order either to decrease the lattice misfit which maintains the coherent interface between precipitate and matrix or to delay the atomic diffusion process during the coarsening process [9]. The chromium addition is expected to increase the high-temperature strength [10] in these ferritic alloys which may help to be used at higher temperatures with a better performance against coarsening. Thus, it is essential to study the coarsening process of this type of alloys.

Therefore the purpose of the present work is to carry out a comparative study of the coarsening process of the $Fe_{0.75}Ni_{0.10}Al_{0.15}$ and $Fe_{0.74}Ni_{0.10}Al_{0.15}Cr_{0.01}$ alloys after aging at temperatures of 750, 850, and 950°C for several times in order to know the effect of the Cr addition on the growth kinetics of coarsening and mechanical properties of this alloy.

2. Experimental Details

Two alloy compositions, $Fe_{0.75}Ni_{0.10}Al_{0.15}$ and $Fe_{0.74}Ni_{0.10}Al_{0.15}Cr_{0.01}$, were melted in an electric arc furnace under an argon atmosphere using high purity Fe (99.9%), Ni (99.99%), Al (99.7%), and Cr (99.9%). The chemical composition of alloys was verified pursuing the chemical analysis by the atomic absorption method with a GBS Avanta equipment based on a variation of ASTM E-353 standard [11] with an experimental error between 0.04 and 0.26% depending on the element. The actual compositions were Fe-10.3at.%Ni-15.2at.%Al and Fe-9.9at.%Ni-15.4at.%Al-1.1at.%Cr, which are very close to the nominal one. The alloy ingots were encapsulated in quartz tube under an argon atmosphere and heated at 1100°C for one week in a tubular electric furnace in order to destroy the as-cast microstructure and homogenize the chemical composition. Specimens of 30 × 30 × 10 mm were cut and encapsulated in a quartz tube under argon atmosphere to conduct the solution treatment at 1100°C for 1 h and then aged at 750, 850, and 950°C for times from 5 to 1000 h. The solution treated and aged specimens were prepared metallographically and etched with an etchant composed of 2 vol.-% nitric acid in methanol and then observed with secondary electron image (SEI) in a JEM 6300 JEOL scanning electron microscope (SEM) equipped with an energy dispersive spectrometer (EDS) at 25 kV. The aged specimens of both alloys were also analyzed by X-ray diffraction analysis with Mo Kα radiation with a Siemens D-5000 equipment in order to confirm the presence of the ordered β' phase. The equivalent circus radius of precipitates r was measured by means of the precipitate area on SEM images with an image analyzing system. In order to get representative data, 200 measurements were done in different zones of the specimens. These measurements mainly corresponded to precipitates with a cuboid morphology. The volume fraction of precipitates was evaluated employing the area method in both the alloy specimens aged at 750, 850, and 950°C for 25, 50, 100, and 200 h. STEM analysis of some aged specimens was carried out with the HAADF detector to obtain a Z-contrast and it was combined with STEM-EDX analysis to know the distribution of chemical elements in matrix and precipitates of some aged specimens. The Vickers hardness, HV 0.1/12 s, was measured in all the aged specimens.

3. Results and Discussion

3.1. Microstructural Evolution of Coarsening. SEM micrographs of the precipitation evolution are shown in Figures 1 and 2(a)–2(d) for the $Fe_{0.75}Ni_{0.10}Al_{0.15}$ and $Fe_{0.74}Ni_{0.10}Al_{0.15}Cr_{0.01}$ alloys, respectively, aged at 750 and 950°C for 50 and 200 h. Both figures show the presence of the β' precipitates in the ferritic matrix. The β' precipitates were confirmed to have the B2 (CsCl) crystalline structure as shown in Figure 3 which shows the superreflections for this phase in both X-ray diffractograms of the alloys aged at 950°C for 50 h. Several diffraction peaks of the β' precipitates are overlapped with those corresponding to the ferrite matrix. The morphology of the β' precipitates is rounded cuboids in both of the aged alloys from the early stages of aging at all temperatures (Figures 1 and 2(a)). The straight sides of precipitates suggest the presence of a coherent interface between precipitates and matrix. The precipitates become aligned with the ferritic matrix over the course of time (Figures 1 and 2(b)). This alignment has been reported [12] to occur in the <100> crystallographic direction of the ferrite matrix since it corresponds to the softest one in the bcc crystalline structure. This suggests that the alloy specimens have the <100> orientation in the aged specimens. A further aging promotes the increase in size of precipitates in both of the aged alloys. The increase in precipitate size is higher as the aging temperature increases. Aging for longer times has a tendency to form square or rectangular arrays of cuboid precipitates in both alloys; however, this fact seems to be higher in the $Fe_{0.75}Ni_{0.10}Al_{0.15}$ alloy aged at 750 and 850°C than that in the other one (Figures 1 and 2(b)). At aging at 950°C, elongated arrays of precipitates are aligned with respect to the ferritic matrix in both alloys (Figures 1 and 2(c)-2(d)). Some coalescence of precipitates is observed in these arrays and the straight sides of some precipitates become curved. This suggests the loss of coherency between the precipitates and matrix. This characteristic is more notorious in the case of the aged $Fe_{0.75}Ni_{0.10}Al_{0.15}$ alloy. This behavior seems to be related to a higher elastic-strain effect in this alloy [13]. No splitting of precipitates was observed to occur in both the aged alloys. The volume fraction of precipitates is also indicated in Figures 1 and 2 and this is, in general, higher for the alloy without chromium; however, the volume fractions are very close in both alloys aged at 750°C.

3.2. Coarsening Growth Kinetics. The average equivalent circus radius, r, of β' precipitates, expressed as r^3, is plotted as a function of aging time in Figure 4 for the aged $Fe_{0.75}Ni_{0.10}Al_{0.15}$ and $Fe_{0.74}Ni_{0.10}Al_{0.15}Cr_{0.01}$ alloys. This figure shows straight line curves for the different cases which suggest that the LSW theory for diffusion-controlled coarsening is followed in this study. The LSW theory and modified LSW theories [1, 2] express mathematically the variation of particle radius with time as follows:

$$r^3 - r_o^3 = k_r t, \tag{1}$$

where r_o and r are the average radius of precipitates at the onset of coarsening and time t, respectively, and k_r is a rate constant which can be determined from the slope of straight lines in Figure 4. The most adequate value of the time exponent n was determined using a regression analysis for each alloy and aging temperature. This indicated that

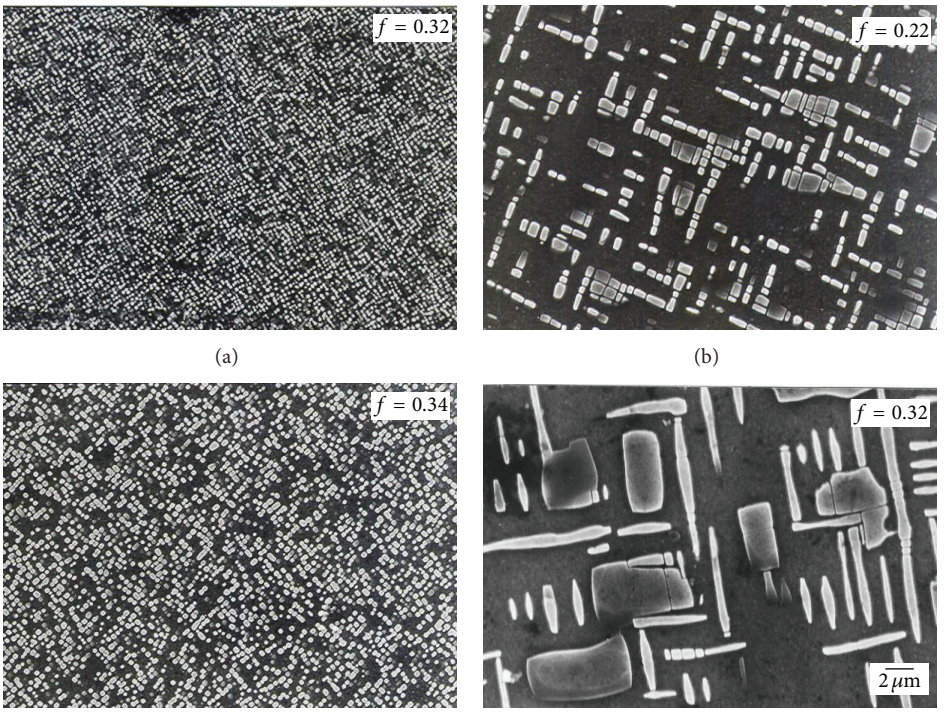

Figure 1: SEM micrographs of the $Fe_{0.75}Ni_{0.10}Al_{0.15}$ alloy aged at (a-b) 750 and (c-d) 950°C for 50 and 200 h, respectively.

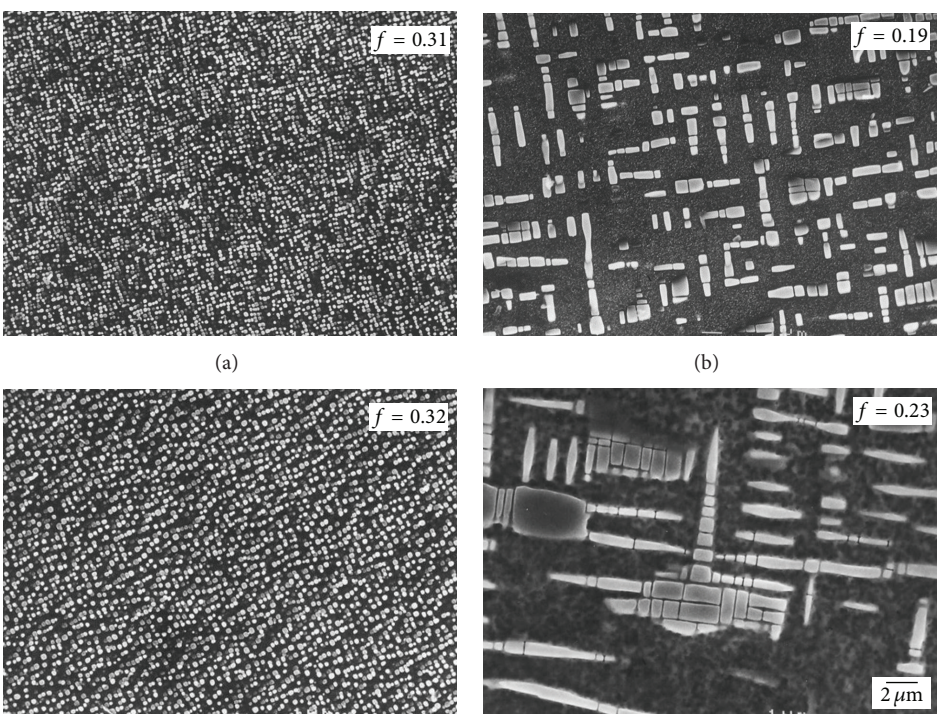

Figure 2: SEM micrographs of the $Fe_{0.74}Ni_{0.10}Al_{0.15}Cr_{0.01}$ alloy aged at (a-b) 750 and (c-d) 950°C for 50 and 200 h, respectively.

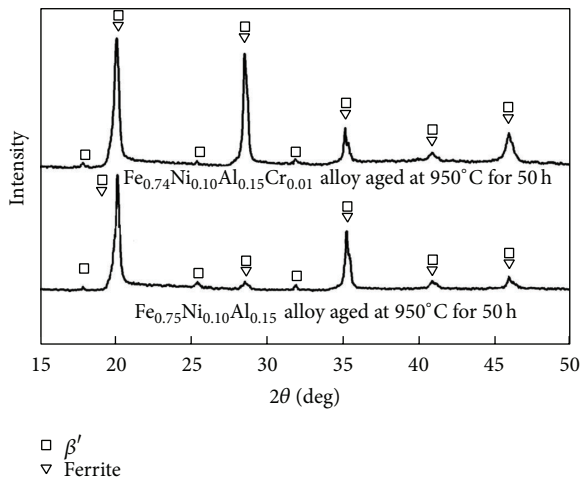

Figure 3: XRD diffractograms of the $Fe_{0.75}Ni_{0.10}Al_{0.15}$ and $Fe_{0.74}Ni_{0.10}Al_{0.15}Cr_{0.01}$ alloys aged at 950°C for 50 h.

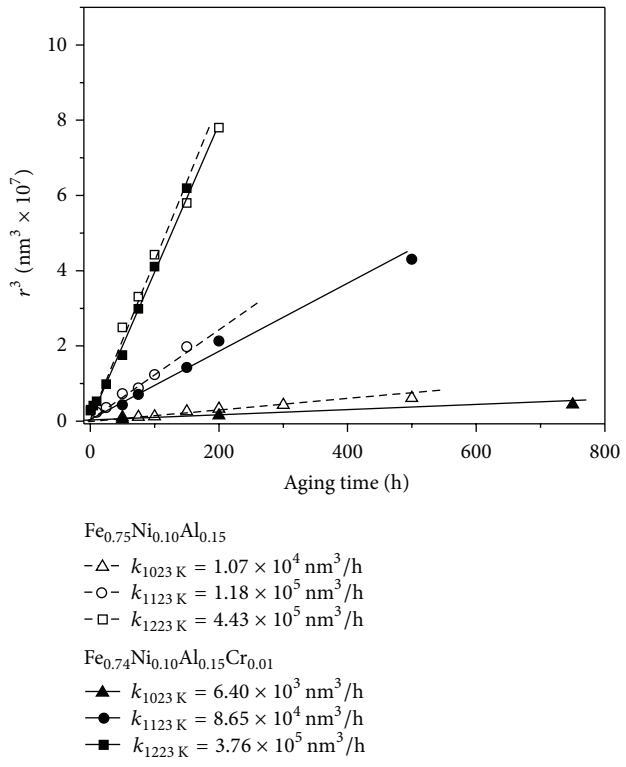

Figure 4: Plot of r^3 value for precipitates against aging time for the aged $Fe_{0.75}Ni_{0.10}Al_{0.15}$ and $Fe_{0.74}Ni_{0.10}Al_{0.15}Cr_{0.01}$ alloys.

the adjusted contribution ratio, R^2, was between 0.964 and 0.993, 0.940 and 0.992, and 0.930 and 0.935 for $n = 3$, 2.5, and 2, respectively, in the ternary alloy. On the other hand, this value was between 0.985 and 0.995, 0.984 and 0.991, and 0.945 and 0.990 for $n = 3$, 2.5, and 2, respectively, in the quaternary alloy. Thus, the highest adjusted contribution ratio R^2 corresponded to the exponent n equal to 3 which is in agreement with the modified LSW theory for diffusion-controlled coarsening.

Figure 4 also shows the values of rate k constant for each case and they indicate that the coarsening process takes place more rapidly for the $Fe_{0.75}Ni_{0.10}Al_{0.15}$ alloy aged at the three temperatures than that of the alloy with the Cr addition in spite of the lower volume fraction of precipitation. Additionally, the activation energy for the coarsening process was determined to be 194 and 212 kJ mol^{-1} for the ternary and quaternary alloys, respectively, using the Arrhenius plot of the rate constant k. The activation energy of the quaternary alloy is higher than that of the ternary alloy which is in agreement with the slower coarsening kinetics observed in the aged $Fe_{0.74}Ni_{0.10}Al_{0.15}Cr_{0.01}$ alloy. Both values of energy are close to the activation energy of 188–234 kJ mol^{-1} reported for the interdiffusion process in Fe-Al alloys [14].

This behavior suggests the effect of chromium on the Ostwald ripening process in this alloy. Figure 5(a) illustrates the HAADF-STEM image of the $Fe_{0.74}Ni_{0.10}Al_{0.15}Cr_{0.01}$ alloy aged at 950°C for 50 h. Some β' precipitates and the ferrite matrix can be observed in the micrograph. The STEM intensity profiles corresponding to Fe, Ni, Al, and Cr elements, following the line from A to B indicated in Figure 5(a), are shown in Figure 5(b). The presence of chromium is slightly higher in the ferrite matrix than that observed in the β' precipitates. The iron content of precipitates is higher than that of nickel and aluminum. In order to show more clearly the effect of alloying elements, a thermo-Calc equilibrium analysis [15] was carried out for the two alloy compositions at temperatures between 750 and 950°C. Thermo-Calc analysis indicates that the ferrite matrix is richer in chromium, about 1.1 at.% for all temperatures, in comparison with that in the β' precipitates. This detail is in good agreement with the chemical behavior reported in the literature for Fe-Ni-Al-Cr alloys [16]. The thermo-Calc calculated mole fraction of alloying elements is shown in Figure 6 for the equilibrium β' phase for the $Fe_{0.75}Ni_{0.10}Al_{0.15}$ and $Fe_{0.74}Ni_{0.10}Al_{0.15}Cr_{0.01}$ alloys at temperatures between 750 and 950°C. These precipitates are expected [17] to be an (Fe, Ni)Al intermetallic compound. Thermo-Calc analysis shows that the iron content in the β' precipitates increases with the aging temperature, from about 10 to 50 at.%, while the nickel and aluminum contents decrease with temperature, from about 45 to 20 at.%, in both alloys. However, the content of iron in the β' precipitates is slightly lower in the $Fe_{0.74}Ni_{0.10}Al_{0.15}Cr_{0.01}$ alloy than that corresponding to the other alloy, while the nickel and aluminum contents of the former alloy are slightly higher than that of the latter alloy. In the case of the alloy with chromium, the chromium contents show a slight increase with temperature, from 0.04 to 0.22 at.%. This chemical behavior suggests that the β' precipitates are an intermetallic compound closer to the NiAl compound in both alloys aged at 750°C since the Fe content is low. In contrast, the β' precipitates are a compound of (Fe, Ni)Al type in both alloys aged at 850 and 950°C showing a considerable amount of iron, which is in good agreement with Figure 5. This behavior may be favorable for having a higher coarsening resistance in these precipitates since the atomic diffusion process would

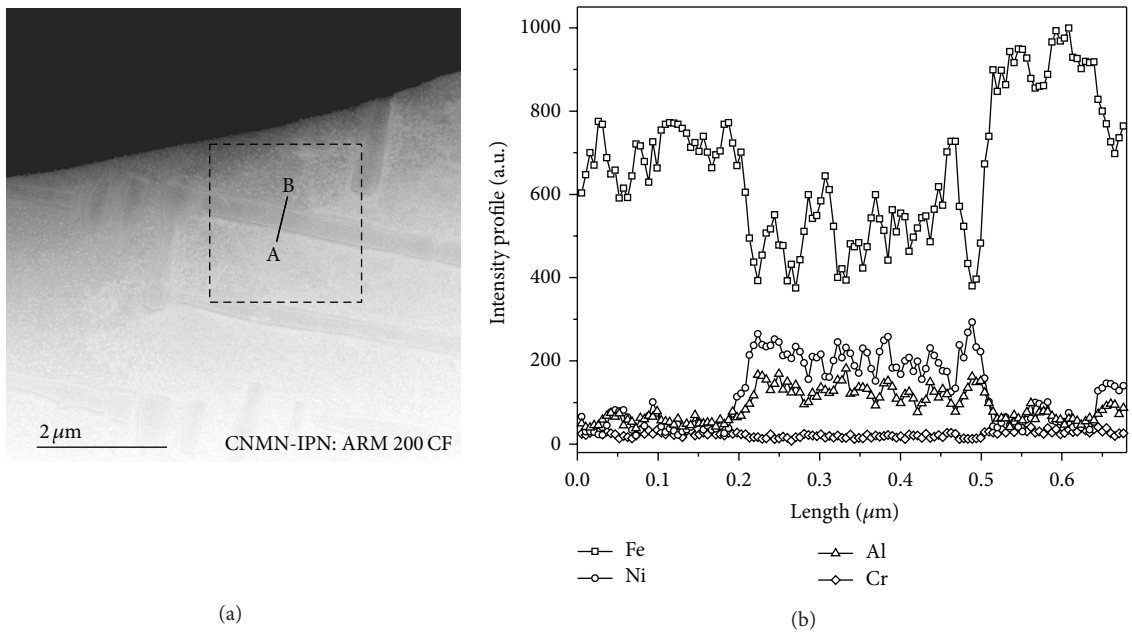

Figure 5: (a) HAADF-STEM image of (Fe, Ni)Al precipitates in a Fe matrix and (b) intensity profile of Fe, Ni, Al, and Cr elements.

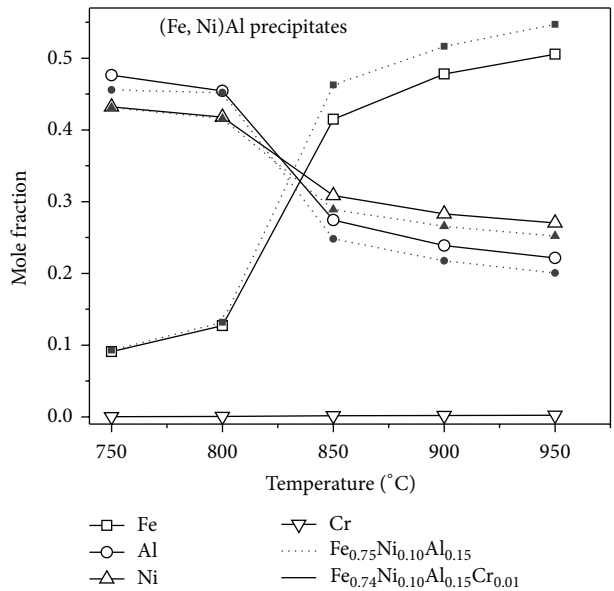

Figure 6: Calculated fraction mole of alloying elements in the β' precipitates against aging temperature for the $Fe_{0.75}Ni_{0.10}Al_{0.15}$ and $Fe_{0.74}Ni_{0.10}Al_{0.15}Cr_{0.01}$ alloys.

be more complex which may cause its retardation [2]. As mentioned above, the coarsening resistance in the alloy with chromium is higher than that observed in the other alloy. This fact can be attributed mainly to the presence of chromium in both the ferrite matrix and β' precipitates which cause a slower diffusion process during the coarsening of precipitates.

The precipitate size distribution, plot of the probability density versus the normalized radius ρ, is shown in Figures 7(a)–7(d) for the $Fe_{0.75}Ni_{0.10}Al_{0.15}$ and $Fe_{0.74}Ni_{0.10}Al_{0.15}Cr_{0.01}$ alloys, respectively, aged at 750°C for 50 and at 950°C for 150 h. The size distribution of the LSW theory for diffusion-controlled coarsening is also shown in these figures. The size distribution of both alloys, aged at 750°C for 50 h (Figures

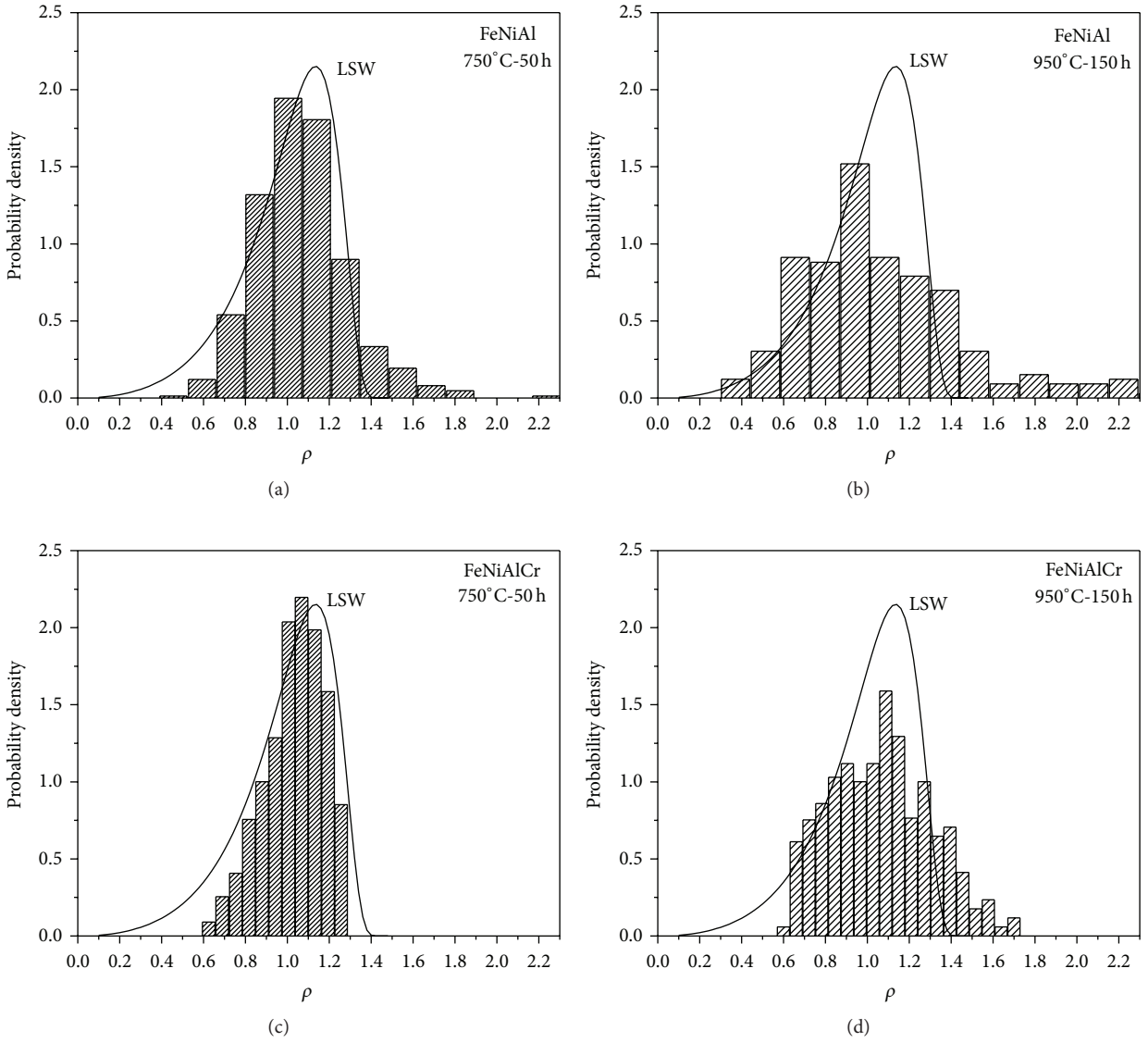

FIGURE 7: Distribution of precipitate size for the (a-b) $Fe_{0.75}Ni_{0.10}Al_{0.15}$ and (c-d) $Fe_{0.74}Ni_{0.10}Al_{0.15}Cr_{0.01}$ alloys aged at 750°C for 50 h and 950°C for 150 h, respectively.

7(a) and 7(c)), is more symmetrical and closer to that one of LSW theory. In contrast, the size distribution of both alloys, aged at 950°C for 150 h (Figures 7(b) and 7(d)), is broader and more symmetrical, which is a coarsening characteristic observed in different binary and ternary alloys, either with large volume fraction of precipitates or with high coherency-elastic strain effect [1, 2].

3.3. Aging Curves. The aging curves are shown in Figure 8 for the two alloys aged at 750, 850, and 950°C. The hardness of $Fe_{0.74}Ni_{0.10}Al_{0.15}Cr_{0.01}$ alloy is higher than that of the $Fe_{0.75}Ni_{0.10}Al_{0.15}$ alloy in spite of the lower volume fraction of precipitates. This higher hardness can be related to the presence of a small amount of chromium in the matrix and precipitates (Figure 6). Besides, the increase in Fe content for the β' precipitates has been reported [18] to cause an increase in strength, while its decrease tends to improve its ductility. The highest resistance to the overaging in these alloys occurs during the aging at 750°C which shows the slowest coarsening kinetics in both alloys. In contrast, the lowest coarsening resistance was observed to take place in the highest aging temperature because of the fastest Ostwald ripening process.

4. Conclusions

The presence of chromium in the $Fe_{0.75}Ni_{0.10}Al_{0.15}$ alloy promotes a higher coarsening resistance of the β' precipitates during aging at temperatures of 750, 850, and 950°C, as well as a higher response to the precipitation hardening. These characteristics can be related to the presence of chromium in both the ferrite matrix and β' precipitates. The chromium addition seems to promote a delay of the precipitate coarsening and an increase in the solution strengthening.

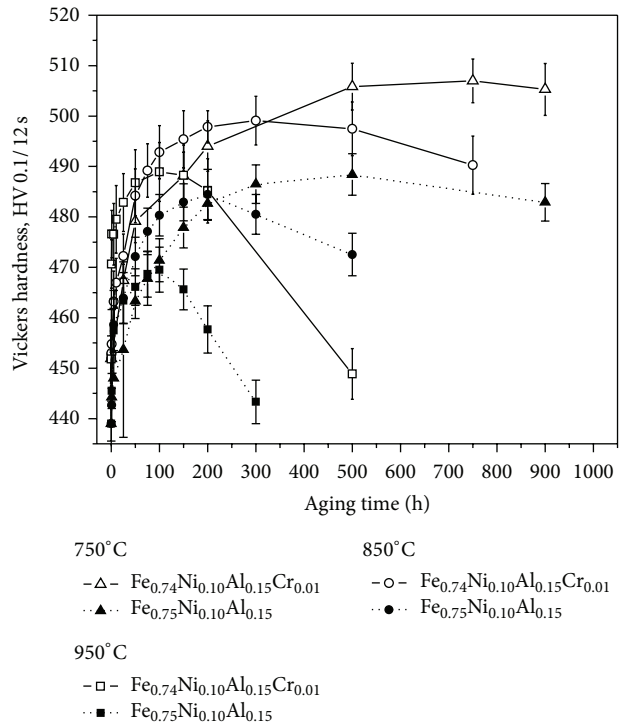

Figure 8: Aging curves for the $Fe_{0.75}Ni_{0.10}Al_{0.15}$ and $Fe_{0.74}Ni_{0.10}Al_{0.15}Cr_{0.01}$ alloys.

Conflict of Interests

The authors declare that there is no conflict of interests regarding the publication of this paper.

Acknowledgments

The authors wish to acknowledge the financial support from SIP-IPN and Conacyt.

References

[1] A. Baldan, "Progress in Ostwald ripening theories and their applications to nickel-base superalloys," *Journal of Materials Science*, vol. 37, no. 11, pp. 2171–2202, 2002.

[2] G. Kostorz, *Phase Transformations in Materials*, Wiley-VCH, Weinheim, Germany, 2nd edition, 2001.

[3] C. J. Kuehmann and P. W. Voorhees, "Ostwald ripening in ternary alloys," *Metallurgical and Materials Transactions A: Physical Metallurgy and Materials Science*, vol. 27, no. 4, pp. 937–942, 1996.

[4] N. Cayetano-Castro, H. J. Dorantes-Rosales, V. M. López-Hirata, J. J. Cruz-Rivera, J. Moreno-Palmerin, and J. L. González-Velázquez, "Coarsening kinetics of coherent precipitates in Fe-10% Ni-15% Al alloy," *Revista de Metalurgia de Madrid*, vol. 44, no. 2, pp. 162–169, 2008.

[5] K. Thornton, N. Akaiwa, and P. W. Voorhees, "Large-scale simulations of Ostwald ripening in elastically stressed solids. I. Development of microstructure," *Acta Materialia*, vol. 52, no. 5, pp. 1365–1378, 2004.

[6] A. J. Ardell, "The effect of volume fraction on particle coarsening: theoretical considerations," *Acta Metallurgica*, vol. 20, no. 1, pp. 61–71, 1972.

[7] M. Schober, C. Lerchbacher, E. Eidenberger, P. Staron, H. Clemens, and H. Leitner, "Precipitation behavior of intermetallic NiAl particles in Fe-6 at.%Al-4 at.%Ni analyzed by SANS and 3DAP," *Intermetallics*, vol. 18, no. 8, pp. 1553–1559, 2010.

[8] G. Sauthoff, *Intermetallics*, Wiley-VCH, New York, NY, USA, 1st edition, 1995.

[9] H. J. Rosales-Dorantes, N. Cayetano-Castro, V. M. Lopez-Hirata, M. L. Saucedo-Muñoz, D. Villegas-Cardenas, and F. Hernández-Santiago, "Coarsening process of coherent β' precipitates in Fe-10wt.%Ni-15wt.%Al and Fe-10wt.%Ni-15wt.%Al-1wt.%Cu alloys," *Materials Science and Technology*, vol. 29, pp. 1492–1498, 2013.

[10] M. A. Muñoz-Morris and D. G. Morris, "Microstructure and mechanical behaviour of a Fe-Ni-Al alloy," *Materials Science and Engineering: A*, vol. 444, no. 1-2, pp. 236–241, 2007.

[11] ASTM International, "Standard test methods for chemical analysis of stainless, heat-resisting, maraging, and other similar chromium-nickel-iron alloys," Tech. Rep. ASTM E-353, 2006.

[12] O. Soriano-Vargas, M. L. Saucedo-Muñoz, V. M. Lopez-Hirata, and A. M. Paniagua-Mercado, "Coarsening of $\beta\prime$ precipitates in an isothermally-aged Fe_{75}-Ni_{10}-Al_{15} alloy," *Materials Transactions*, vol. 51, no. 3, pp. 442–446, 2010.

[13] A. Baldan, "Progress in Ostwald ripening theories and their applications to the γ'-precipitates in nickel-base superalloys Part II: Nickel-base superalloys," *Journal of Materials Science*, vol. 37, no. 12, pp. 2379–2405, 2002.

[14] H. Mehrer, *Diffusion in Solid Metals and Alloys*, Springer, Berling, UK, 1st edition, 1990.

[15] Thermo-Cal software v. 3.1/Niv5.TDB, 2008.

[16] C. Stallybrass and G. Sauthoff, "Ferritic Fe-Al-Ni-Cr alloys with coherent precipitates for high-temperature applications," *Materials Science and Engineering A*, vol. 387–389, no. 1-2, pp. 985–990, 2004.

[17] C. Stallybrass, A. Schneider, and G. Sauthoff, "The strengthening effect of (Ni,Fe)Al precipitates on the mechanical properties at high temperatures of ferritic Fe-Al-Ni-Cr alloys," *Intermetallics*, vol. 13, no. 12, pp. 1263–1268, 2005.

[18] I. M. Anderson, A. J. Duncan, and J. Bentley, "Site-distributions of Fe alloying additions to B2-ordered NiAl," *Intermetallics*, vol. 7, no. 9, pp. 1017–1024, 1999.